NANO LETTERS

Letter

pubs.acs.org/NanoLett

Integrated High-Quality Factor Optical Resonators in Diamond

B. J. M. Hausmann,[†,⊥] I. B. Bulu,[†,⊥] P. B. Deotare,[§,⊥] M. McCutcheon,[§] V. Venkataraman,[†] M. L. Markham,[∥] D. J. Twitchen,[∥] and M. Lončar[†,*]

[†]School of Engineering and Applied Sciences, Harvard University, Cambridge, Massachusetts 02138, United States

[§]Department of Electrical Engineering and Computer Science, Massachusetts Institute of Technology, Cambridge, Massachusetts 02139, United States

[§]Lux Research, Boston, Massachusetts 02110, United States

[∥]Element Six Ltd, King's Ride Park, Ascot SL5 8BP, United Kingdom

ABSTRACT: The realization of an integrated diamond photonic platform, based on a thin single crystal diamond film on top of a silicon dioxide/silicon substrate, is reported. Using this approach, we demonstrate high-quality factor single crystal diamond race-track resonators, operating at near-infrared wavelengths (1550 nm). The devices are integrated with low-loss diamond waveguides terminated with polymer pads (spot size converters) to facilitate in- (out-) coupling of light from (to) an optical fiber. Optical characterization of these resonators reveal quality factors as high as ~250 000 and overall insertion losses as low as 1 dB/facet. Scattering induced mode splitting as well as signatures of nonlinear effects such as optical bistability are observed at an input pump power of ~100 mW in the waveguides.

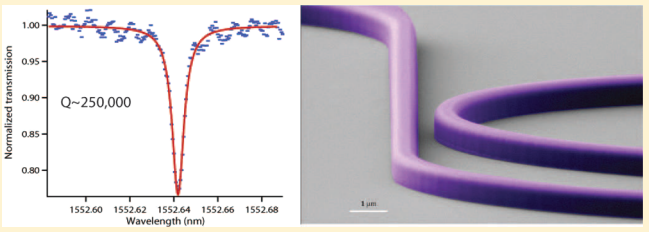

KEYWORDS: *diamond, resonators, nano photonics, integrated optics*

Unique material properties make diamond a promising candidate for on-chip high-performance photonic devices with novel functionalities. In particular, diamond's large Raman-gain[1] (13.5 cm/GW at 1064 nm), relatively large Kerr nonlinearity[2] (n_2 = 1.3 × 10^{-15} cm^2/W), wide bandgap (~5.5 eV), negligible multiphoton loss mechanisms,[3] as well as excellent thermal properties (high thermal conductivity of 2000 W/mK, and small thermo-optic coefficient of (dn/dT) = 10 × 10^{-6} K^{-1})[4] are of interest for the implementation of active and passive optical devices capable of handling high optical powers. In order to take full advantage of these exceptional properties of diamond, it is desirable to fabricate devices integrated on a chip. A diamond-on-insulator (DOI) platform recently developed for applications in quantum optics,[5] based on single crystal diamond films on top of a low index substrate, is well suited for these applications. Two promising applications of DOI, and diamond photonics in general, are the realization of coherent light sources based on Raman scattering at wavelengths where semiconductor lasers are hard to implement,[6] and parametric nonlinear processes that may lead to wide-bandwidth frequency comb generation.[7]

However, the realization of high-performance devices places stringent requirements on the diamond film quality. For example, polycrystalline diamond approaches[8] suffer from light absorption and scattering at grain boundaries, and therefore single-crystal diamond films are of interest for applications mentioned above. Single-crystal thin diamond films can be generated using either ion implantation assisted liftoff[9] or substrate thinning approaches.[5b,c,10] The former method leaves residual stress within the diamond films[11] that can be detrimental for applications in photonics, but might be overcome using an approach based on regrowth of diamond.[12] This makes the latter approach the most promising route towards a high-performance DOI platform so far and is the one employed in this work. However, further advances in material science and engineering will likely overcome difficulties associated with polycrystalline and ion-sliced single crystal diamond films. For example, low-loss optical waveguides and resonators having high quality (Q) factors have been successfully fabricated in other polycrystalline materials including Si[13] and TiO_2,[14] while ion-slicing is routinely used for high-performance silicon-on-insulator (SOI) platforms.

To design waveguide coupled single crystal diamond (SCD) ring resonators based on the DOI platform, 3D Finite difference time domain (FDTD) modeling (Lumerical Solutions, Inc.) is used. The coupling efficiency between the waveguide and the ring resonator is determined by their cross sections and separation (the gap size). For example, single mode operation is obtained at 1,550 nm for a diamond waveguide with a cross-section of 600 nm × 500 nm (refractive index n_{diam} of 2.4) on a 2 μm thick SiO_2 on Si substrate capped with silica. The coupling Q-factor between waveguide and cavity is larger than 250 000 for a gap size of 500 nm. A resonator length of ~330 μm is used.

Received: October 8, 2012
Revised: February 14, 2013
Published: February 21, 2013

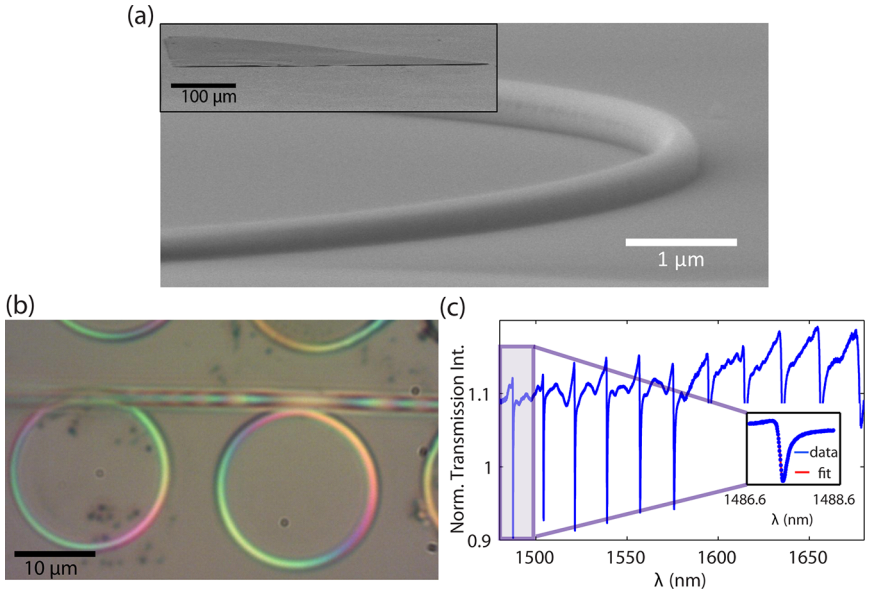

Figure 1. (a) Scanning electron microscopy (SEM) image of a diamond ring resonator on low index substrate. The residual resist layer remained on the ring during characterization. Inset: SEM image of an optically thin single crystal diamond slab on a SiO_2/Si substrate before making devices. (b) Optical image of single diamond ring resonators on a quartz substrate. A tapered optical fiber, used to in- and out-couple light, can also be seen. The rings have a 20 μm diameter with a waveguide cross-section of 410 nm × 1 μm. The 300 nm thick low-index (~1.5) resist layer was kept on top of the ring. The rainbow-pattern in the rings is due to thickness variations of the diamond film. (c) Transmission measurement features sharp dips that correspond to the modes of the ring resonator. The *Q*-factors obtained using Fano-like fits range from 700 (1678 nm) to 9000 (1487 nm). Inset: Blow-up of one of the resonances.

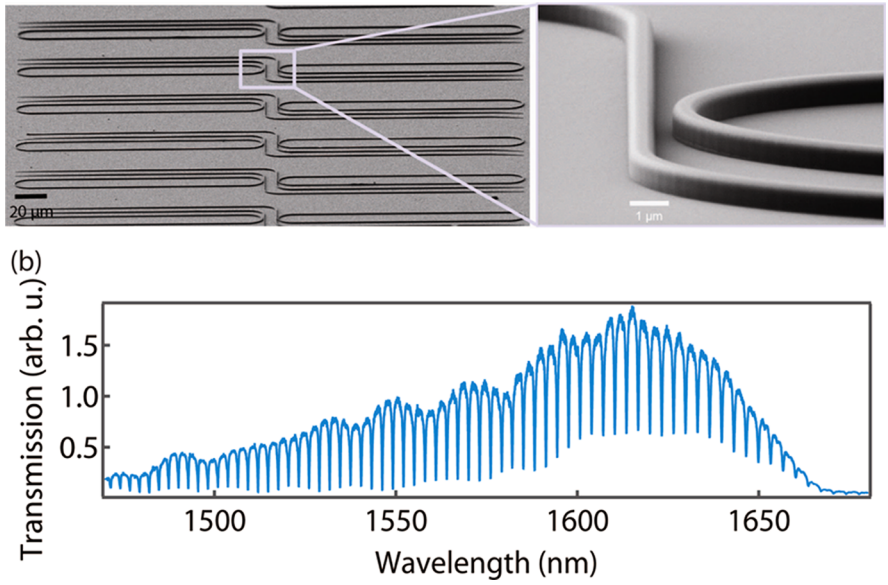

Figure 2. (a) SEM micrograph of an array of diamond racetrack resonators (330 μm length) coupled to diamond waveguides. Coupling polymer pads are not shown here. Inset: Close-up of the waveguide-resonator coupling region. The height, width, and gap size of the devices are in the range of 600−700 nm, 550−650 nm, and 450−500 nm, respectively. (b) Transmission spectrum obtained from a 314 μm long race-track resonator. *Q*-factors as high as 30000 are observed for devices without silica top cladding.

To test our predictions, an array of bare diamond ring resonators without coupling waveguides and capping silica are first fabricated on quartz substrates. A slightly different geometry from the one discussed above is used with an outer ring radius of 20 μm and cross section of 400 nm × 1 μm. The fabrication sequence used is similar to the one developed by HP[5c] and us[5b] and has been reasonably successful for the generation of quantum-optical devices in diamond. Briefly, a 20 μm thick type Ib SCD slab (Element Six) is thinned to a desired device layer thickness, by an oxygen-based inductively coupled plasma reactive ion etch (ICP RIE) (see inset scanning electron microscope (SEM) image of Figure 1a). An etch mask is formed by performing e-beam lithography (Elionix) using XR-1541−6 e-beam resist (spin-on-glass, Dow Corning), which is then transferred to the diamond film in a second etch step (see ring profile in Figure 1a). The fabricated rings are shown in Figure 1b along with the tapered silica fiber[15] which is used to evanescently couple light to the rings. To ensure coupling to

dx.doi.org/10.1021/nl3037454 | *Nano Lett.* 2013, 13, 1898−1902

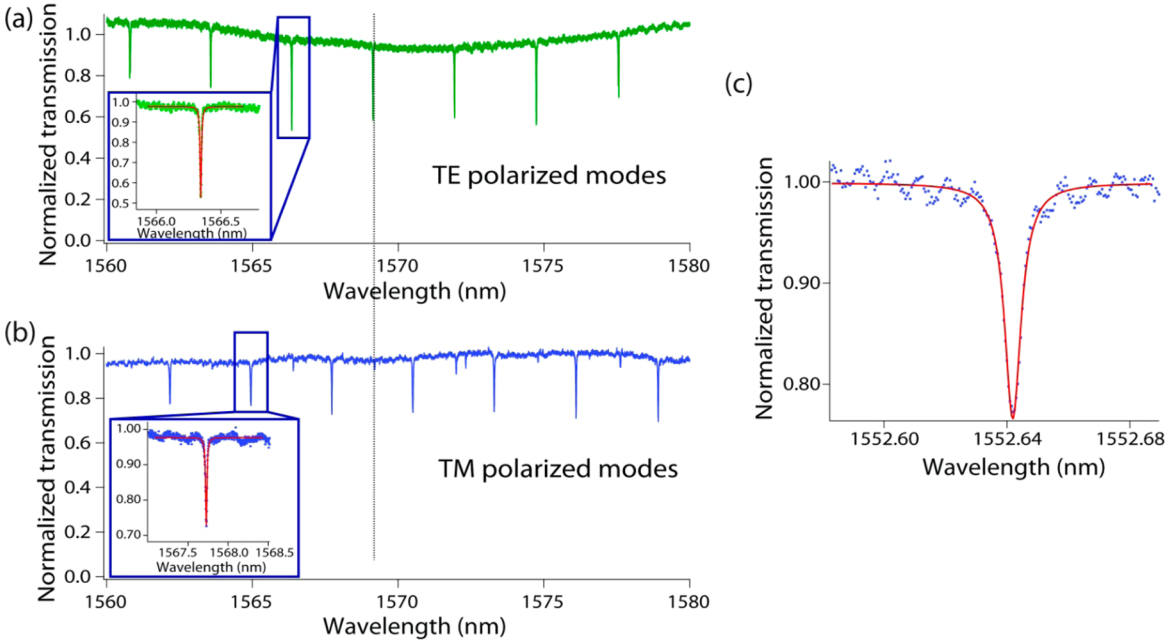

Figure 3. *Q*-factor of racetrack resonators can be increased by capping them with SiO_2 (deposited by PECVD). Both TE and TM modes are supported, as shown in (a) and (b) respectively. Lorentzian fits reveal *Q*-factors of ∼125 000 for TE modes and ∼76 000 for TM modes. (c) The highest *Q*-factor measured (TE resonance) is ∼250 000.

one device at a time, a small dimple is indented in the middle of the tapered region.[16] Note that in the experiments presented here the optical fiber is in contact with the diamond rings. The performance of the ring resonators is probed in transmission measurements using scanning lasers (Santec, TSL 510) spanning a 1480−1680 nm wavelength range.

Figure 1c shows a representative normalized transmission spectrum, which features regularly spaced dips that correspond to optical resonances of the structure. The inset in Figure 1c shows a blow-up of one of the resonances, which has been fitted to a Fano profile[17]

$$F(\lambda) = a_1 - a_2 \cdot \frac{\left(q + \frac{2(\lambda - \lambda_0)}{\gamma}\right)^2}{1 + \left(\frac{2(\lambda - \lambda_0)}{\gamma}\right)^2}$$

Here, γ corresponds to the linewidth of the resonance while λ_0 represents the resonant wavelength. The asymmetry of the resonance is attributed to the Fano parameter q[17b] while a_1, a_2 are fitting parameters. The Fano-like shape is attributed to interference between light coupled to the ring resonator and light partially reflected from fiber discontinuities (e.g., fiber-ring coupling section, fiber facets), which leads to a perturbation of the phase of the transmitted wave.[18] A *Q*-factor of ∼9000 at λ = 1487.4 nm is extracted, corresponding to a finesse (F) of ∼100. Both quantities decrease significantly for longer wavelengths (Q ∼ 700, F ∼ 12 for λ = 1676 nm), which is attributed to a larger scattering loss at the outer ring edge caused by reduced confinement in the high index material, as well as to larger coupling into the fiber. Because the fiber is touching the ring resonator, the measurements are likely performed in the overcoupled limit where the field decay rate to the tapered fiber exceeds the intrinsic loss rate of the ring resonator, thus reducing the overall *Q*-factor of the resonator. This effect is more dramatic at long wavelengths where the transmission drops by only 18% on resonance.

The color change in the optical image (Figure 1b) is attributed to the thickness variation of the film, which arises from the polishing step. A wedgelike profile of the diamond plates has been measured prior fabrication with a minimum of 1 μm thickness change over a 3 mm sample.

To realize fully integrated diamond photonic networks that enable efficient and robust coupling of light into the cavity, we replace the tapered optical fiber with diamond waveguides fabricated in close proximity to the ring and racetrack resonators (Figure 2). In addition, polymer in and out-coupling pads consisting of SU-8 resist with a 3 μm × 3 μm cross-section are defined in a second e-beam lithography step to extend the diamond waveguides to both ends of the sample. This procedure improves the coupling between an optical (lensed) fiber to the on-chip diamond waveguide.[19] To ensure optimal coupling between the diamond waveguide and the polymer pads the diamond waveguides are adiabatically tapered. Figure 2a shows a SEM image of a representative diamond race-track resonator on a SiO_2/Si substrate with extended diamond waveguides.

Lensed fibers (Oz optics) are used to couple light into and out of the cleaved facets of the device. An outline of the experimental setup and the butt-coupling technique used here are described in detail by Deotare et al.[19] A transmission spectrum of a typical ring resonator device, shown in Figure 2b, reveals resonator modes with *Q*-factors as high as 30 000. In this case, an overall transmission loss of 12 dB is inferred. To further improve the coupling efficiency as well as increase the cavity Q factor, a 2 μm thick SiO_2 layer is deposited on top of our devices (after polymer pads are defined) using plasma enhanced chemical vapor deposition (PECVD). A different sample from the one shown in Figure 2a was used here with a 330 μm resonator length. After cleaving, the sample facets are polished to maximize the fiber-coupling and to avoid any scrambling of polarization due to facet imperfections. Using this approach an order of magnitude increase in coupling efficiency

dx.doi.org/10.1021/nl3037454 | *Nano Lett.* 2013, 13, 1898−1902

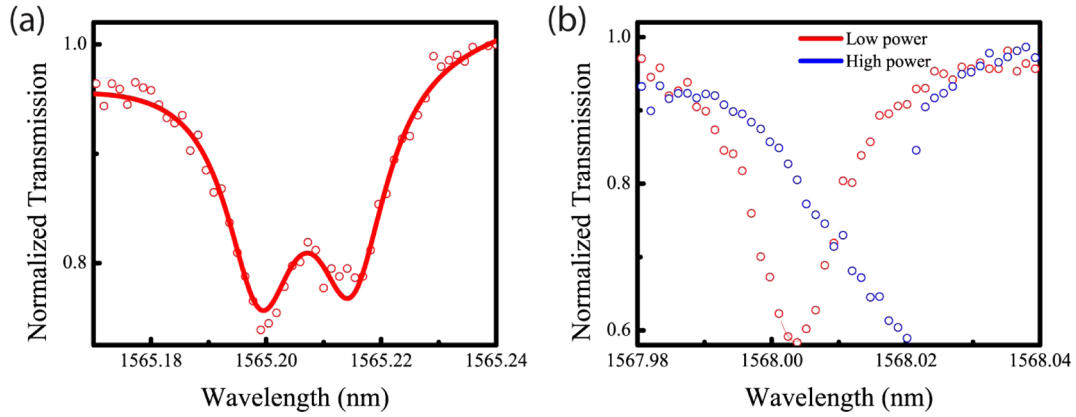

Figure 4. (a) Mode splitting is observed, indicative of coupling between clockwise and counter-clockwise traveling modes due to scattering. (b) Nonsplit mode of the same device at low (red) and high (blue) pump powers shows signature of optical bistability at high pump powers.

is observed, and an overall transmission loss down to 2 dB (1 dB/facet) is inferred for the best device. Both TE and TM modes are identified withTE modes usually having higher *Q*-factors than TM modes (Figure 3 panels a,b, respectively). *Q*-factors as high as $\sim 2.5 \times 10^5$ are obtained from fits to the experimental data. The increase in *Q*-factor is attributed to the reduced scattering losses resulting from the reduced index contrast between the diamond core and the silica cladding. We estimate the waveguide propagation loss[20] to be 1.7 dB/cm from transmission data (*Q*-factor and on-resonance transmission dip), assuming undercoupled devices. Since this estimation accounts for scattering, absorption, and bending losses of the ring, it provides an upper limit for the diamond waveguide propagation loss.

To confirm the values of *Q*-factors reported above, the input laser is phase modulated with a 3 GHz sine wave to generate sidebands in the laser spectrum at known frequency spacing. These sidebands provide a "ruler" against which measured resonant linewidths are compared.[21] Using this precise approach we infer that the *Q*-factors reported above are underestimated by 7%.

Scattering along the resonator's surfaces or inside the diamond ring can cause the initially degenerate counter-propagating modes to couple, which is referred to as intracavity backscattering.[22] The characteristic signature of this intermode coupling is the splitting of the modes as seen in Figure 4a. The response of the system can be analyzed by the following set of coupled mode equations[22c]

$$\frac{da_+}{dt} = -\left(\frac{\gamma_t}{2} + i\Delta\omega_0\right)a_+ + i\beta a_- + \kappa s$$

$$\frac{da_-}{dt} = -\left(\frac{\gamma_t}{2} + i\Delta\omega_0\right)a_- + i\beta a_+$$

where $a_\pm$ represent the amplitudes of clock-wise and counter-clockwise ring resonator modes, γ_t is the decay rate, β is the coupling rate between the two modes, s is the amplitude of the input pump field in the coupling waveguide, and κ is the coupling rate between the waveguide and the resonator. The detuning between excitation and resonance frequency (of the degenerate mode) is denoted as $\Delta\omega_0$. The observed splitting in the modes is most likely caused by scattering due to fabrication imperfections. Further improvements in fabrication, and e-beam lithography in particular, should eliminate the splitting and also result in higher *Q*-factors.

Finally, we observed the signatures of optical bistability in our devices for large input powers (Figure 4b). With increasing input power the cavity resonance shows a characteristic bistable line shape with a red shift and a steep drop-off as the laser is scanned from lower to higher wavelengths. The bistability threshold power is estimated to be ~100 mW inside the waveguide for a device with a *Q*-factor of 1.22×10^5. The observed nonlinearity stems most likely from a combination of the optical Kerr effect (intensity dependent refractive index) due to the $X^{(3)}$ nonlinearity of diamond, and the thermo-optic effect originating from the surrounding silica. Time-dependent studies, beyond the scope of the current manuscript, will provide more insight to the origin of nonlinearity.[23] We do note, however, that the wide bandgap of diamond makes nonlinear effects due to multiphoton absorption that plagues Si photonics at telecom wavelengths highly unlikely. Similarly, free-carrier dispersion is not a likely origin for the nonlinear effects. The thermal contributions can be suppressed by using a substrate with higher thermal conductivity than silica.

In conclusion, the operation of high-*Q* diamond race-track resonators integrated with low-loss diamond waveguides at telecom wavelengths is demonstrated. The integrated diamond photonic platform presented here is the first step toward integrated frequency combs and Raman lasers based on diamond. Owing to diamond's large linear and nonlinear refractive index thresholds for parametric oscillation[24] and Raman lasing to be 300 mW and 10 mW, respectively, for existing devices with optimal geometries having *Q*-factors of 250 000. Optimization of the fabrication method and waveguide−ring coupling section will result in a higher coupling efficiency and in a higher optical power transfer from the waveguide to the ring thus further increasing the efficiency of our device.

AUTHOR INFORMATION

Corresponding Author

*E-mail: loncar@seas.harvard.edu.

Author Contributions

⊥B.J.M.H., I.B.B., and P.B.D. contributed equally to this paper.

Notes

The authors declare no competing financial interest.

ACKNOWLEDGMENTS

Devices were fabricated in the Center for Nanoscale Systems (CNS) at Harvard. B.H. gratefully acknowledges support from

the Harvard Quantum Optics Center (HQOC). This work was supported in part by NSF and AFOSR MURI (Grant FA9550-12-1-0025). M.L. acknowledges support from the Sloan Foundation.

REFERENCES

(1) Feve, J.-P. M.; Shortoff, K. E.; Bohn, M. J.; Brasseur, J. K. High average power diamond Raman laser. *Opt. Exp.* **2011**, *19* (2), 913.

(2) Boyd, R. W. *Nonlinear Optics*, 3rd ed.; Academic Press: New York, 2008.

(3) Dadap, J. I.; Focht, G. B.; Reitze, D. H.; Downer, M. C. Two-photon absorption in diamond and its application to ultraviolet femtosecond pulse-width measurement. *Opt. Lett.* **1991**, *16* (7), 499–501.

(4) Nebel, C.; Ristein, J. *Semiconductors and Semimetals: Thin-Film Diamond I*; Elsevier Academic Press: New York, 2004.

(5) (a) Loncar, M.; Babinec, T.; Choy, J.; Hausmann, B.; Bulu, I.; Zhang, Y.; Khan, M.; McCutcheon, M. W. Diamond Nanophotonics and Quantum Optics. In *Artificial Atoms in Diamond: From Quantum Physics to Applications*; Cambridge, MA, Nov. 11–13, 2010. (b) Hausmann, B. M.; Shields, B. J.; Quan, Q.; Maletinsky, P.; McCutcheon, M. W.; Choy, J. T.; Babinec, T. M.; Kubanek, A.; Yacoby, A.; Lukin, M. D.; Loncar, M. Integrated diamond networks for quantum nanophotonics. *Nano Lett.* **2012**, *12* (3), 1578. (c) Faraon, A.; Barclay, P. E.; Santori, C.; Fu, K.-M. C.; Beausoleil, R. G. Resonant enhancement of the zero-phonon emission from a colour centre in a diamond cavity. *Nat. Photonics* **2011**, *5*, 301.

(6) (a) Spillane, S. M.; Kippenberg, T. J.; Vahala, K. J. Ultralow-threshold Raman laser using a spherical dielectric microcavity. *Nature* **2002**, *415*, 621. (b) Rong, H.; Jones, R.; Liu, A.; Cohen, O.; Hak, D.; Fang, A.; Paniccia, M. A continuous-wave Raman silicon laser. *Nature* **2005**, *433*, 725. (c) Rong, H.; Xu, S.; Kuo, Y.-H.; Sih, V.; Cohen, O.; Raday, O.; Paniccia, M. Low-threshold continuous-wave Raman silicon laser. *Nat. Photonics* **2007**, *1*, 232. (d) Mildren, R. P.; Butler, J. E.; Rabeau, J. R. CVD-diamond external cavity Raman laser at 573nm. *Opt. Express* **2008**, *16* (23), 18950.

(7) (a) Zhi, M.; Wang, X.; Sokolov, A. V. Broadband coherent light generation in diamond driven by femtosecond pulses. *Opt. Express* **2008**, *16* (16), 12139. (b) Del'Haye, P.; Schliesser, A.; Arcizet, O.; Wilken, T.; Holzwarth, R.; Kippenberg, T. J. Optical frequency comb generation from a monolithic microresonator. *Nature* **2007**, *450*, 1214–1217.

(8) (a) Wang, C. F.; Choi, Y.-S.; Lee, J. C.; Hu, E. L.; Yang, J.; Butler, J. E. Observation of whispering gallery modes in nanocrystalline diamond microdisks. *Appl. Phy. Lett.* **2007**, *90*, 081110. (b) Wang, C. F.; Hanson, R.; Awschalom, D. D.; Hu, E. L. Fabrication and characterization of two-dimensional photonic crystal microcavities in nanocrystalline diamond. *Appl. Phy. Lett.* **2007**, *91*, 201112. (c) Hiscocks, M. P.; Ganesan, K.; Gibson, B. C.; Huntington, S. T.; Ladouceur, F.; Prawer, S. Diamond waveguides fabricated by reactive ion etching. *Opt. Express* **2009**, *16* (24), 19512–19519.

(9) (a) Wang, C. F.; Hu, E. L.; Yang, J.; Butler, J. E. Fabrication of suspended single crystal diamond devices by electrochemical etch. *J. Vac. Sci. Technol., B* **2007**, *25*, 730–733. (b) Lee, J. C.; Aharonovich, I.; Magyar, A. P.; Rol, F.; Hu, E. L. Coupling of silicon-vacancy centers to a single crystal diamond cavity. *Opt. Exp.* **2012**, *20* (8), 8891. (c) Parikh, N. R.; Hunn, J. D.; McGucken, E.; Swanson, M. L.; White, C. W.; Rudder, R. A.; Malta, D. P.; Posthill, J. B.; Markunas, R. J. Single crystal diamond plate liftoff achieved by ion implantation and subsequent annealing. *Appl. Phys. Lett.* **1992**, *61*, 3124.

(10) Faraon, A.; Santori, C.; Huang, Z.; Acosta, V. M.; Beausoleil, R. G. Coupling of Nitrogen-Vacancy Centers to Photonic Crystal Cavities in Monocrystalline Diamond. *Phys. Rev. Lett.* **2012**, *109*, 033604.

(11) Magyar, A. P.; Lee, J. C.; Limarga, A. M.; Aharonovich, I.; Rol, F.; Clarke, D. R.; Huang, M.; Hu, E. L. Fabrication of thin, luminescent, single-crystal diamond membranes. *Appl. Phys. Lett.* **2011**, *99*, 081913.

(12) Aharonovich, I.; Lee, J. C.; Magyar, A. P.; Buckley, B. B.; Yale, C. G.; Awschalom, D. D.; Hu, E. L. Homoepitaxial Growth of Single Crystal Diamond Membranes for Quantum Information Processing. *Adv. Mater.* **2012**, *24*, OP54.

(13) Preston, K.; Schmidt, B.; Lipson, M. Polysilicon photonic resonators for large-scale 3D integration of optical networks. *Opt. Express* **2007**, *15* (25), 17283.

(14) Bradley, J. D. B.; Evans, C. C.; Choy, J. T.; Reshef, O.; Deotare, P. B.; Parsy, F.; Phillips, K. C.; Loncar, M. M. E. Submicrometer-wide amorphous and polycrystalline anatase TiO_2 waveguides for microphotonic devices. Submitted for publication.

(15) (a) Knight, J. C.; Cheung, G.; Jacques, F.; Birks, T. A. Phase-matched excitation of whispering-gallery-mode resonances by a fiber taper. *Opt. Lett.* **1997**, *22* (15), 1129. (b) Cai, M.; Painter, O.; Vahala, K. J. Observation of Critical Coupling in a Fiber Taper to a Silica-Microsphere Whispering-Gallery Mode System. *Phys. Rev. Lett.* **2000**, *85* (1), 74–77.

(16) (a) Barclay, P. E.; Srinivasan, K.; Borselli, M.; Painter, O. Probing the dispersive and spatial properties of photonic crystal waveguides via highly efficient coupling from fiber tapers. *App. Phys. Lett.* **2004**, *85* (1), 4. (b) Srinivasan, K.; Barclay, P. E.; Borselli, M.; Painter, O., Optical-fiber-based measurement of an ultrasmall volume high-Q photonic crystal microcavity. *Phys. Rev. B* **2004**, *70*.

(17) (a) Galli, M.; Portalupi, S. L.; Belotti, M.; Andreani, L. C.; O'Faolain, L.; Krauss, T. F. Light scattering and Fano resonances in high-Q photonic crystal nanocavities. *Appl. Phys. Lett.* **2009**, *94*, 071101. (b) Fano, U. Effects of Configuration Interaction on Intensities and Phase Shifts. *Phys. Rev. Lett.* **1961**, *124*, 1866.

(18) Chao, C.-Y.; Guo, L. J. Biochemical sensors based on polymer microrings with sharp asymmetrical resonance. *Appl. Phys. Lett.* **2003**, *83* (8), 1527.

(19) Deotare, P. B.; Bulu, I.; Frank, I. W.; Quan, Q.; Zhang, Y.; Ilic, R.; Loncar, M. Broadband Reconfiguration of OptoMechanical Filters. *Nat. Commun.* **2012**, *3*, 846.

(20) Luo, L.-W.; Wiederhecker, G. S.; Cardenas, J.; Poitras, C.; Lipson, M. High quality factor etchless silicon photonic ring resonators. *Opt. Express* **2011**, *19* (7), 6284.

(21) Collot, L.; Lefevre-Seguin, V.; Brune, M.; Raimond, J. M.; Haroche, S. Very High-Q Whispering-Gallery Mode Resonances Observed on Fused Silica Microspheres. *Europhys. Lett.* **1993**, *23* (5), 327.

(22) (a) Gorodetsky, M. L.; Ilchenko, V. S. Thermal nonlinear effects in optical whispering-gallery microresonators. *Laser Phys. Rev.* **1992**, *2*, 1004. (b) Gorodetsky, M. L.; Pryamikov, A. D.; Ilchenko, V. S. Rayleigh scattering in high-Q microspheres. *J. Opt. Soc. Am. B* **2000**, *17* (6), 1051. (c) Kippenberg, T. J.; Spillane, S. M.; Vahala, K. J. Modal coupling in traveling-wave resonators. *Opt. Lett.* **2002**, *27* (19), 1669. (d) Borselli, M.; Johnson, T. J.; Painter, O. Beyond the Rayleigh scattering limit in high-Q silicon microdisks: theory and experiment. *Opt. Express* **2005**, *13* (5), 1515.

(23) Shankar, R.; Bulu, I.; Leijssen, R.; Loncar, M. Study of thermally-induced optical bistability and the role of surface treatments in Si-based mid-infrared photonic crystal cavities. *Opt. Express* **2011**, *19* (24), 24828.

(24) Herr, T.; Hartinger, K.; Riemensberger, J.; Wang, C. Y.; Gavartin, E.; Holzwarth, R.; Gorodetsky, M. L.; Kippenberg, T. J. Universal formation dynamics and noise of Kerr-frequency combs in microresonators. *Nat. Photonics* **2012**, *8*, 480.